Journal of Biomolecular NMR (2006) 34: 75–87
DOI 10.1007/s10858-005-5582-7
© Springer 2006

Article

^{13}C, ^{15}N Resonance assignment of parts of the HET-s prion protein in its amyloid form

Ansgar B. Siemer[a], Christiane Ritter[b], Michel O. Steinmetz[c], Matthias Ernst[a], Roland Riek[b] & Beat H. Meier[a,*]

[a]*Physical Chemistry, ETH Zurich, CH-8093, Zurich, Switzerland;* [b]*Structural Biology Laboratory, The Salk Institute, La Jolla, CA 92037, USA;* [c]*Biomolecular Research, Structural Biology, Paul Scherrer Institut, CH-5232, Villigen, PSI Switzerland*

Received 12 August 2005; Accepted 18 November 2005

Key words: amyloid, HET-s, prions, solid-state NMR

Abstract

The partial ^{15}N and ^{13}C solid-state NMR resonance assignment of the HET-s prion protein fragment 218–289 in its amyloid form is presented. It is based on experiments measured at MAS frequencies in the range of 20–40 kHz using exclusively adiabatic polarization-transfer schemes. The resonance assignment within each residue is based on two-dimensional $^{13}C—^{13}C$ correlation spectra utilizing the DREAM mixing scheme. The sequential linking of the assigned residues used a set of two- and three-dimensional $^{15}N—^{13}C$ correlation experiments. Almost all cross peaks visible in the spectra are assigned, but only resonances from 43 of the 78 amino-acid residues could be detected. The missing residues are thought to be highly disordered and/or highly dynamic giving rise to broad resonance lines that escaped detection in the experiments applied. The line widths of the observed resonances are narrow and comparable to line widths observed in micro-crystalline samples. The 43 assigned residues are located in two fragments of about 20 residues.

Abbreviations: 2D – two-dimensional; 3D – three-dimensional; APHH – adiabatic-passage Hartmann-Hahn; CP – cross polarization; CW – continuous wave; DREAM – dipolar recoupling enhanced by amplitude modulation; HORROR – homonuclear rotary resonance; MAS – magic angle spinning; NMR – nuclear magnetic resonance; NOE – nuclear overhauser effect; PDSD – proton-driven spin diffusion; R^2T – rotational resonance tickling; RFDR – radio-frequency driven spin diffusion; TPPI – time-proportional phase increment; TRIS – tris(hydroxymethyl)aminomethane; XiX – X inverse X.

Introduction

Solid-state NMR spectroscopy of proteins has become an interesting tool for structural biology due to the recent development of methods for resonance assignment, distance measurements, and determination of torsion angles. Increasing resolution due to higher static magnetic fields, improved decoupling techniques, advanced sample preparation, and higher MAS frequencies make it now possible to investigate systems with roughly 100 amino-acid residues. These developments have led to the first resonance assignments of proteins and protein domains (Pauli et al., 2001), (van Rossum et al., 2003), (Bockmann et al., 2003), (Igumenova et al., 2004b), (Igumenova et al., 2004a), (Gammeren et al., 2005) as well as to

*To whom correspondence should be addressed. E-mail: beme@ethz.ch

three-dimensional structures (Jaroniec et al., 2004), (Castellani et al., 2002), (Castellani et al., 2003), (Lange et al., 2005), (Zech et al., 2005) determined by solid-state NMR. Solid-state NMR requires no long-range order in the sample and it is possible to investigate nano- and micro-crystalline, fibrous, and membrane proteins at atomic resolution given that the spectral resolution is sufficient.

Sequential resonance assignment is one of the prerequisites for atomistic structure determination by NMR. Several strategies for the ^{15}N and ^{13}C assignment of peptides and proteins using solid-state NMR techniques have been developed in the last few years (Petkova et al., 2003), (Detken et al., 2001), (Rienstra et al., 2000), (Ishii and Tycko, 2000), (Hong, 1999), (Straus et al., 1998). For the identification of the ^{13}C resonances within a residue, broadband recoupling methods are usually applied (Bennett et al., 1992), (Brinkmann et al., 2000), (Carravetta et al., 2000), (Verel et al., 1998), (Verel et al., 2001), (Baldus and Meier, 1996). For the sequential assignment of the amino-acid residues, two- and three-dimensional correlation experiments are applied which make use of heteronuclear transfer by cross-polarization (CP) and homonuclear transfer by broad-band (vide supra) and narrow-band dipolar recoupling schemes such as rotational-resonance tickling (R^2T) (Takegoshi et al., 1995), (Takegoshi et al., 1997), (Costa et al., 1997).

In this work we present the partial ^{15}N and ^{13}C resonance assignment of the HET-s prion protein fragment 218–289 in its fibrillized state. The HET-s protein of the fungus *Podospora anserina* is involved in a genetically controlled programmed cell death phenomenon termed heterokaryon incompatibility (Glass et al., 1997), (Saupe, 2000). The HET-s protein occurs in two different forms, a non-prion and a prion form. Strains expressing HET-s in the non-prion form [Het-s*] can undergo a transition to the prion state [Het-s] by contact with [Het-s] strains and by introduction of recombinant HET-s fibrils (Maddelein et al., 2002). The prion form aggregates *in vivo* (Coustou-Linares et al., 2001) and recombinant HET-s amyloid fibrils form spontaneously *in vitro* (Dos Reis et al., 2002). The C-terminal fragment 218–289 which forms the protease-resistant part of these fibrils has the sequence: KI DAIVGRNSAK DIRTEERARV QLGNVVTAAA LHGGIRISDQ TTNSVETVVG KGESRVLIGN EYGGKGFWDN. This fragment also forms amyloid fibrils *in vitro* and when injected into the fungus generates the prion phenotype (Balguerie et al., 2003). The resonance assignment presented in this work shows which parts of the fibril are rigid and well ordered.

Materials and methods

Sample preparation

$^{13}C/^{15}N$-labeled HET-s(218–289) with a C-terminal His Tag was expressed as described for other HET-s constructs (Balguerie et al., 2003). The bacterial pellets were dissolved and sonicated in 6 M guanidium hydrochloride containing 50 mM TRIS pH 8.0 and 150 mM sodium chloride. The supernatant was cleared by centrifugation for 30 min at $18{,}000\times g$. The protein was purified from the supernatant by HIS_6-affinity chromatography and concentrated to approximately 0.5–1 mM. Fast buffer exchange to 50 mM TRIS pH 8.0 containing 150 mM sodium chloride yielded HET-s(218–289), which started to aggregate immediately into amyloid fibrils.

The fibrils were washed in H_2O and centrifuged into the MAS rotor. At no step, the sample was dried or lyophillized. Both drive tip and endcap were sealed using two-component epoxy adhesive (Araldit, Vantico AG). For the assignment, two samples in 1.8 and 2.5 mm rotors were prepared. The two samples were obtained from different production batches but turned out two give identical results for all experiments performed. The filling weight of the 2.5 mm rotor was 14 mg. The dry weight of protein is below this value considering the gel-like nature of the sample. The fibrils used for electron microscopy come from the batch used to fill the 2.5 mm rotor (just before the final centrifugation step). The temperature-dependent NMR spectra were recorded on an additional sample prepared in a water-glycerol (1:1 by volume) mixture and centrifuged into a 2.5 mm rotor.

NMR-spectroscopy

All spectra were recorded on a Bruker AV600 spectrometer operating at a static field of 14.09 T. For MAS frequencies above 30 kHz a home-build 1.8 mm triple-resonance MAS probe (Samoson et al., 2005) was used. For all other measurements a Chemagnetics/Varian 2.5 mm triple-resonance

T3 probe was used. The samples were cooled to temperatures of 5–15 °C. ^{13}C spectra were calibrated using adamantane as an external reference (Earl and VanDerHart, 1982), (Morcombe and Zilm, 2003). The ^{15}N shifts were calibrated indirectly to adamantane with a ^{15}N to $^{1}H_{TMS}$ frequency ratio of $\Xi = 0.10132912$ (Harris et al., 2002), yielding ^{15}N shifts relative to liquid ammonia.

The experimental details for the pulse sequences used in this study (see Figure 1) have been collected in Tables A and B of the supplementary material (available on the web). The pulse sequences are built up from modular building blocks combined in different ways to produce the desired polarization-transfer pathway as schematically depicted in Figure 1. Heteronuclear polarization transfer was implemented using adiabatic-passage Hartmann-Hahn cross-polarization (APHH CP) (Hediger et al., 1994), (Hediger et al., 1995), (Baldus et al., 1996) either to generate the initial polarization ($^{1}H—^{13}C$ or $^{1}H—^{15}N$) or as a polarization-transfer step in a heteronuclear correlation experiment ($^{15}N—^{13}C$) employing simultaneous cw decoupling on the protons. Proton decoupling during all free evolution periods was implemented using the XiX scheme (Detken et al., 2002). Broad-band homonuclear polarization transfer used the DREAM scheme (Verel et al., 1998), (Verel et al., 2001). Narrow-band homonuclear polarization transfer employed the rotational-resonance tickling (R^2T) method (Takegoshi et al., 1995), (Takegoshi et al., 1997), (Costa et al., 1997), (Detken et al., 2001). Sign-discrimination in the indirect dimensions was accomplished using TPPI (Marion and Wuthrich, 1983).

The experimental scheme used for recording $^{13}C—^{13}C$ correlation spectra is shown in Figure 1a. The polarization transfer is based on the adiabatic DREAM scheme (Verel et al., 1998), (Verel et al., 2001). Spectra recorded at 25 kHz MAS were optimized for recoupling the aliphatic region by setting the ^{13}C carrier frequency in the center of the aliphatic region, corresponding to 44.9 ppm. Spectra at 40 kHz MAS used a ^{13}C transmitter frequency of 72.9 ppm to optimize the transfer from the aliphatic region to C′. By changing the direction of the sweep (up-down or down-up) different polarization-transfer pathways, especially for multi-step transfers, can be enhanced or suppressed (vide infra).

NCA and NCO $^{15}N—^{13}C$ triple-resonance correlation spectra were recorded with the double APHH-CP scheme of Figure 1b (Baldus et al., 1996). The second CP step was implemented frequency-selectively (Baldus et al., 1998) with a low rf-field amplitude on the ^{13}C channel and a carrier frequency in the desired spectral region (for numerical values see Table A of the supplementary material). For the NCA and NCO experiments at 25 kHz MAS the carrier frequencies of the ^{13}C channel were set to 44.3 ppm (NCA) and 162.4 ppm (NCO), respectively. For the experiments at 40 kHz MAS the ^{13}C carrier frequencies were 61.4 ppm (NCA) and 172.3 ppm (NCO).

Figure 1c depicts the pulse scheme for N(CA)CB spectra (Detken et al., 2001), and variables are specified in Table B of the supplementary material. The selective CP step was the same as in the NCA experiments at 25 kHz MAS. The relay polarization transfer was accomplished using a DREAM sequence optimized for the aliphatic region by setting the ^{13}C carrier frequency at 44.3 ppm in the center of the aliphatic region.

The N(CO)CA experiment at 20 kHz MAS was done with the pulse sequence shown in Figure 1d (Detken et al., 2001). Parameters are specified in table B of the supplementary material. During the $^{15}N—^{13}C$ cross-polarization step, the ^{13}C channel was set to 169.7 ppm to achieve selective polarization transfer to the carbonyl region. During the relay R^2T polarization-transfer step the carrier was set to 114.6 ppm. The R^2T used a 'ramp-in' pulse followed by a tangential sweep through the rotational-resonance condition in the tilted frame and a 'ramp-out' pulse. By introducing an additional indirect dimension, as illustrated in Figure 1d, the same experiment can also be recorded as a 3D $^{15}N—^{13}C—^{13}C$ correlation experiment. Because the R^2T polarization-transfer step between C^{α} and C′ at 14.09 T is only feasible at MAS frequencies around 20 kHz, the N(CO)CA experiment at 40 kHz was done with the pulse sequence shown in Figure 1c. For this experiment the same selective polarization-transfer was used as for the NCO experiment at 40 kHz MAS. The relay polarization transfer used a DREAM recoupling step.

The N(CA)CO spectrum at 40 kHz MAS was recorded using the pulse sequence shown in Figure 1c (see also Table B of the supplementary material) with ^{13}C carrier frequencies set to

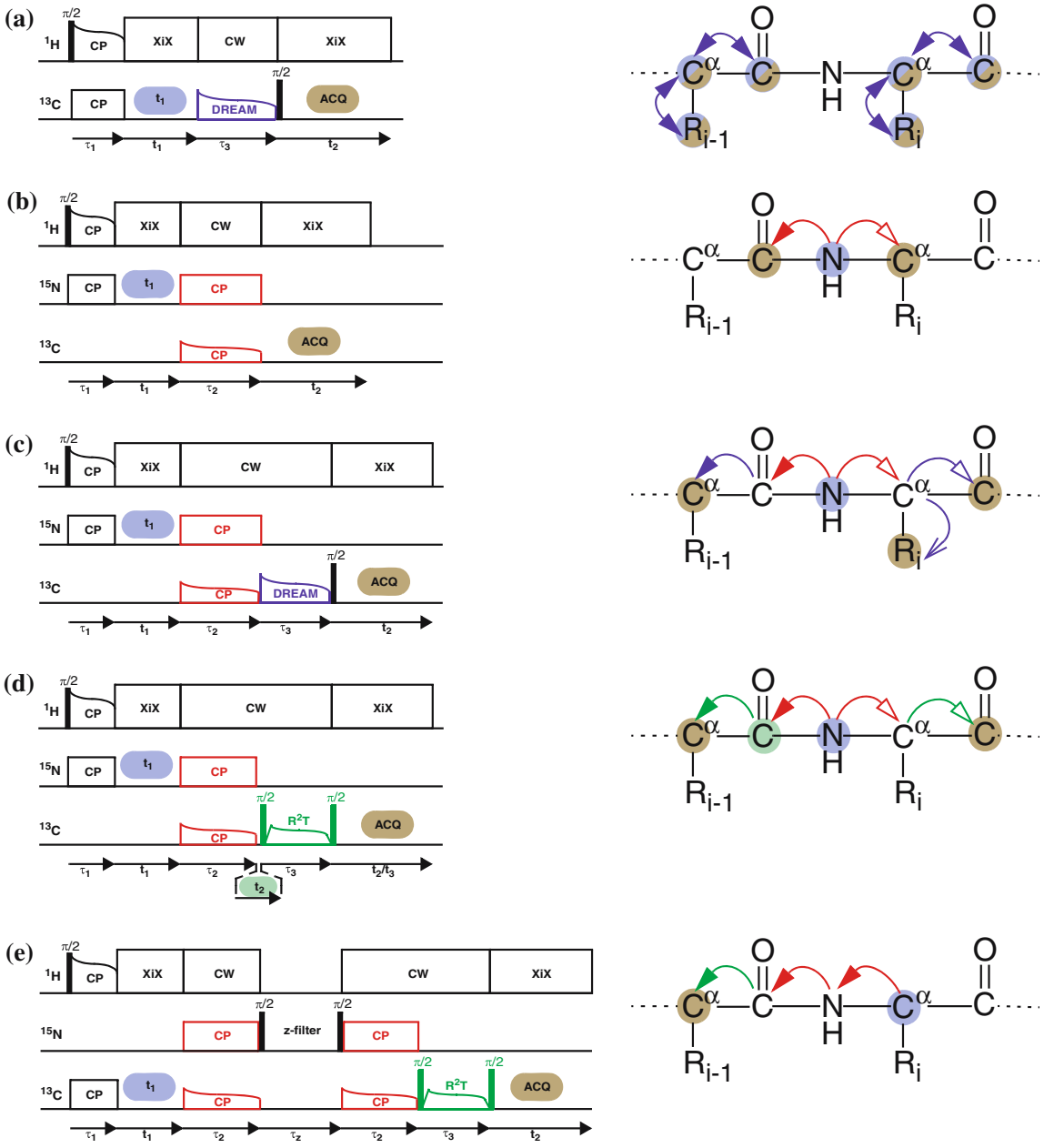

Figure 1. Schematics of the pulse sequences used in the assignment of the resonances and schematic drawings of the polarization-transfer pathway in the protein backbone and side chain. Indirect and direct detection are highlighted with the same colors as the corresponding sites in the peptide. Polarization transfers are indicated with arrows in the same colors as the corresponding building-block in the sequence. Different arrow styles illustrate alternative polarization-transfer pathways. (a) DREAM pulse sequence used for the homonuclear ^{13}C—^{13}C correlations spectra. (b) Double APHH CP experiment for direct ^{15}N —^{13}C correlation. The second CP was done with low rf-field amplitudes on the ^{13}C channel in order to get selective transfer from N_i to either C'_{i-1} or C^{α}_{i}. (c) Double APHH CP experiment followed by a homonuclear DREAM recoupling step. Depending on the frequency of the ^{13}C channel during the second CP and the choice of the HORROR condition, this sequence was used for N(CA)CB, N(CO)CA and N(CA)CO experiments. (d) Double APHH CP with subsequent R^2T recoupling. This sequence was used for a N(CO)CA experiment setting the ^{13}C carrier to the C′ region during the second CP. This sequence was used also to record a NCOCA 3D experiment by introducing an additional ^{13}C evolution period. (e) Pulse sequence for the CA–CA experiment. This sequence consists of three APHH CP's followed by a R^2T recoupling step. The first CP to ^{13}C was done with high rf-amplitudes. The second and third CP were done with low rf-amplitudes on ^{13}C to ensure frequency selectivity.

Table 1. ^{13}C and ^{15}N chemical shifts of the HET-s fragment 218–289 in ppm referenced to TMS and liquid ammonia respectively

Res.	N	C′	C^{α}	C^{β}	C^{γ}	C^{δ}	$N^{\delta/\varepsilon/\zeta}$
ASN226	125.5	–	49.9	37.9	174.6		–
SER227	119.2	169.9	54.7	65.0			
ALA228	122.7	174.9	47.4	21.6			
LYS229	123.6	–	57.7	30.4	23.2	27.5	–
ASP230	117.7	–	51.1	43.1	–		
ILE231	122.7	172.6	58.9	39.5	25.3/15.4	11.8	
ARG232	129.8	–	52.1	30.7	–	–	–
THR233	113.5	172.5	57.6	69.7	21.5		
GLU234	120.0	171.8	51.7	31.7	33.8	180.8	
GLU235	117.3	172.2	56.6	25.2	36.3	182.7	
ARG236	122.8	174.3	52.6	28.4	26.2	41.6	85.2
ALA237	126.0	173.9	51.1	17.7			
ARG238	117.9	172.7	52.9	33.2	24	39.2	–
VAL239	122.7	171.1	58.0	34.7	20.2/18.6		
GLN240	126.7	171.1	50.7	30.7	29.4	173.5	104.4
LEU241	131.4	–	50.6	42.5	25.5	–	
GLY242	113.7	168.7	41.8				
ASN243	109.9	174.3	49.2	38.1	174.2		–
VAL244	122.8	172.5	60.0	32.3	22.4/19.9		
VAL245	129.3	–	59.2	29.9	20.3/18		
THR246	116.7	173.3	60.4	68.8	18.8		
ALA247	121.1	177.4	54.1	14.8			
ALA248	119.3	177.6	53.0	16.1			
ASN262	128.2	–	50.3	38.9	174.5		–
SER263	117.6	169.8	54.3	64.0			
VAL264	125.6	172.5	55.0	33.4	20.9/18.5		
GLU265	127.3	174.0	57.4	27.4	35.1	181.6	
THR266	112.8	171.0	58.9	69.6	20.0		
VAL267	124.1	–	58.5	33.4	–		
VAL268[a]	128.6	173.2	59.2	32.0	18.6		
GLY269	113.4	170.0	42.5				
LYS270	121.5	174.7	52.3	33.2	22.1	27.5	88.5
GLY271	115.6	170.1	46.4				
GLU272	128.6	174.3	52.1	27.8	35.2	182.8	
SER273	116.3	171.5	57.2	64.6			
VAL275	122.9	170.7	58.2	33.9	20.8/19.5		
LEU276	130.6	–	50.6	41.5	24.6	21.8/24	
ILE277	130.3	171.3	56.6	33.5	24/16.5	12.3	
GLY278	111.3	170.0	41.9				
ASN279	114.5	171.0	49.8	38.4	175.6		115.4
GLU280	120.4	–	52.6	31.4	35.7	179.7	
TYR281	128.9	174.4	54.0	38.3	–	–	
GLY282	109.9	172.3	44.0				

[a]The $C^{\gamma 1}$ and $C^{\gamma 2}$ chemical shifts of Val268 are degenerated.

45.2 ppm during the selective CP step to C^{α} and during the DREAM sweep to optimize the polarization transfer to the C′ region.

The 2D CA–CA correlation experiment was recorded with the pulse sequence of Figure 1e at a MAS frequency of 20 kHz (see also Table B of the

supplementary material). The second and third CP step were implemented as selective transfers from C^{α} to N (^{13}C carrier frequency was set to 66.3 ppm) and N to C′ (carrier was shifted to 172.3 ppm). The z-filter between the second and third CP step was used for pathway selection. For the R^2T transfer step, the ^{13}C carrier was set to 112.7 ppm, roughly the center between the C^{α} and C′ regions.

Data procession and data analysis

All spectra were processed using the XWINNMR software package (Bruker-Biospin). The homonuclear ^{13}C—^{13}C correlation spectra were Fourier transformed using a cosine-square window function with zero filling to 2048 data points in both dimensions. The 2D heteronuclear ^{15}N—^{13}C correlation spectra were obtained using a cosine-square window function with zero filling to 2 k data points in t_2 and 256 data points in t_1. The 3D heteronuclear ^{15}N—^{13}C—^{13}C correlation spectrum was Fourier transformed using cosine-square window function with zero filling to 2 k data points in t_3 and 64 and 128 data points in t_1 and t_2, respectively. The resonance assignment was carried out using the program CARA (Keller, 2004) (http://www.nmr.ch).

Electron microscopy

For negative staining, sample aliquots of 5 µl were applied to a weakly glow-discharged carbon coated 400-mesh/inch copper grid. The sample was allowed to adsorb for 30 s, washed twice with water, and negatively stained for 20 s with 2% (w/v) uranyl acetate. Specimens were examined in a Philips Morgagni transmission electron microscope operated at 80 kV. Micrographs were recorded with a Megaview III CCD camera at a nominal magnification of 50,000×.

Results and discussion

Quality of spectra

The line width of the ^{13}C resonances observed in the homonuclear chemical-shift correlation spectra (Figure 3) was typically between 0.25 and 1 ppm and, therefore, comparable to ^{13}C line width observed in micro-crystalline proteins (Igumenova et al., 2004a), (Castellani et al., 2003). No optimization of the preparation for linewidth was performed but we noticed that dried samples gave rise to much broader lines. Our spectra gave no hints for peak doubling and the atomic structure of the fibrils (e.g. the register of the beta sheets) seems to homogenous which is in contrast to observations in other fibrillar systems.

These well resolved spectra came somewhat as a surprise in light of the quite heterogeneous appearance of the fibrillized sample in electron micrographs and comparing them to those observed in other amyloid fibrils (Tycko, 2004) (Petkova et al., 2004) (Jaroniec et al., 2004). As shown in Figure 2, negatively stained HET samples inspected by transmission electron microscopy (TEM) revealed non-branched fibres ~6 nm in diameter (upper panel) that laterally associate to form thick bundles (lower panel). Processing the NMR spectra without line broadening imposed by an apodization function results in fully or partially resolved J splitting for some of the C′—C^{α} cross peaks (Siemer et al., 2005). Typical ^{13}C line width in spectra processed with line broadening are in the order of 0.5–1 ppm. This clearly indicates that the assigned part of the HET-s fibrils are very well ordered and homogeneous on a molecular scale. Seemingly, heterogeneous bundling of fibrils does not compromise the line width. Although the 1.8 and 2.5 mm rotors contained fibrils coming from different batches, no difference in line-position was observed between those and no significant differences in line width were found.

Assignment strategy

Despite the relatively narrow line widths, our spectra suffered from partially severe overlap especially when C′, having a very small chemical-shift dispersion, was involved. The assignment process, therefore, required an iterative strategy taking into account the information from the entire range of spectra described in Figure 1. The following general description of the assignment strategy should be understood as a general outline of the main strategies.

In a first step, spin systems (each corresponding to one residue) were identified by resolved C^{β}—C^{α} cross peaks in the aliphatic region using the

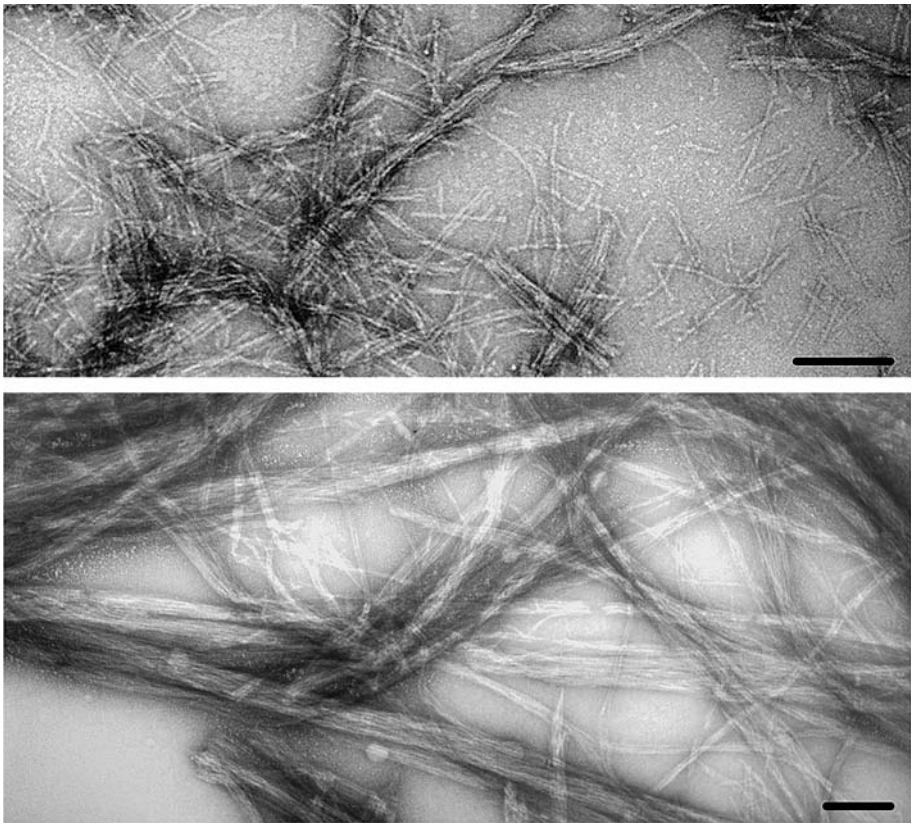

Figure 2. TEM micrographs of negatively stained HET-s(218–289). Fibrils were branched off the sample which was centrifuged into the 2.5 mm MAS rotor. Scale bars denote 100 nm.

^{13}C—^{13}C DREAM correlation spectrum recorded at 25 kHz MAS (Figure 3b). The side-chain resonances belonging to the spin system picked were assigned afterwards using the same spectrum. By identifying the characteristic cross-peak patterns many of the spin systems could be assigned to amino-acid types already at that stage. The DREAM spectrum shows not only correlations between directly bonded spins as strong negative peaks (red contours), but also multi-step correlations over two to three ^{13}C—^{13}C bonds within a given amino acid residue.

In a next step of the assignment process, C′ carbons were assigned to a spin systems via C^{α}—C′ and C^{β}—C′ correlations in the carbonyl region of a ^{13}C—^{13}C DREAM correlation spectrum (Figure 3a) recorded at 40 kHz MAS. During the DREAM recoupling scheme the HORROR condition for each spin pair is matched at different times during the rf-amplitude sweep (Verel et al., 2001). Therefore, depending on the order of the sequential passing of the individual recoupling conditions involved in a relayed transfer, some polarization-transfer pathways are possible while others are not. In the 40 kHz experiment, for example, the order of transitions for typical values of C′, C^{α} and C^{β} resonances is C^{α}—C′ before C^{α}—C^{β} in the low-to-high-amplitude sweep and C^{α}—C^{β} before C^{α}—C′ in the high-to-low-amplitude sweep. The low-high sweep will have strong C^{α}—*C′* cross peaks (with negative intensity) whereas the high-low sweep will feature strong C^{β}—C′ relayed cross-peaks with positive sign of the cross peak intensity, respectively. The former are poorly resolved as can be seen from Figure 3a. Hence most of C′ spins were assigned via the C^{β}—C′ correlations and the N(CA)CO spectrum as discussed below.

The backbone nitrogen resonances were assigned to the corresponding spin system via the N—C^{α} and N—C^{x} (where x denotes side-chain ^{13}C atoms) cross-peaks in the NCA and N(CA)CB

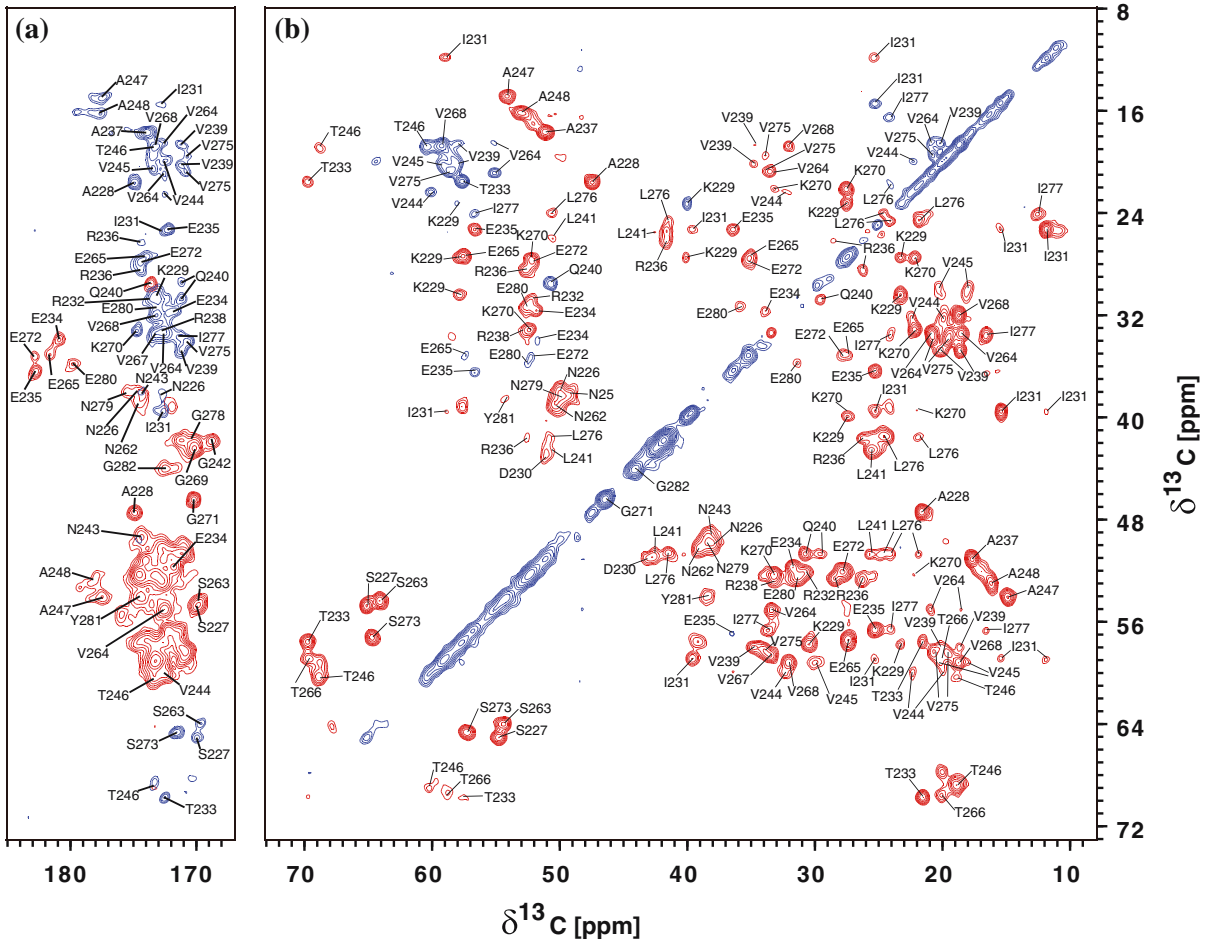

Figure 3. Homonuclear ^{13}C DREAM spectra of HET-s(218–289). The lowest level of the contours was chosen just above the noise level. The factor between the contour level was 1.4 for all 2D spectra presented in this publication. (a) Carbonyl region of the DREAM spectra recorded at 40 kHz MAS. Positive contours (blue) were taken from a spectrum recorded with a high-to-low-amplitude tangential DREAM sweep, negative contours were taken from a similar spectrum but with a low-to-high sweep. Contours start at 5% of the minimum intensity. (b) Aliphatic region of a DREAM spectrum recorded at 25 kHz MAS. Positive contours are shown in blue, negative contours in red. Contours start at 3% of the maximal intensity.

spectra, respectively. The NCA spectrum recorded at 40 kHz MAS is shown in Figure 4b. Based on this spectrum eight nitrogen resonances could be assigned unequivocally. The rest of the backbone nitrogens were assigned via the N(CA)CB spectrum recorded at 25 kHz MAS (Figure 5). In this spectrum not only N—C^{β} but also correlations between the backbone ^{15}N resonances and other side-chain ^{13}C resonances are visible. Two examples of these are the well resolved Lys229 NC^{γ} and Ile231 N—$C^{\delta 1}$ cross peaks which are highlighted in Figure 5. It was possible to assign a backbone ^{15}N resonance for virtually all spin systems. The N(CA)CO Spectrum recorded at 40 kHz MAS (Figure 4a) was used to confirm these ^{15}N assignments via the N—C′ cross-peaks or, if the ^{15}N assignment was unambiguous, to assign the C′ resonance in the spin system.

Knowing the backbone ^{15}N resonance it is possible to assign a C'_{i-1} and C^{α}_{i-1} resonances for each spin system by evaluating the NCO and the N(CO)CA spectra. This step was rather ambiguous because for many ^{15}N chemical shifts several possible C'_{i-1},C^{α}_{i-1} pairs could be found. For example, the amino acids Ala228, Ile231, Arg236, Val239, Val244, Val275 have almost the same ^{15}N chemical shift as can be seen from the N(CO)CA spectrum shown in Figure 6a. Another problem

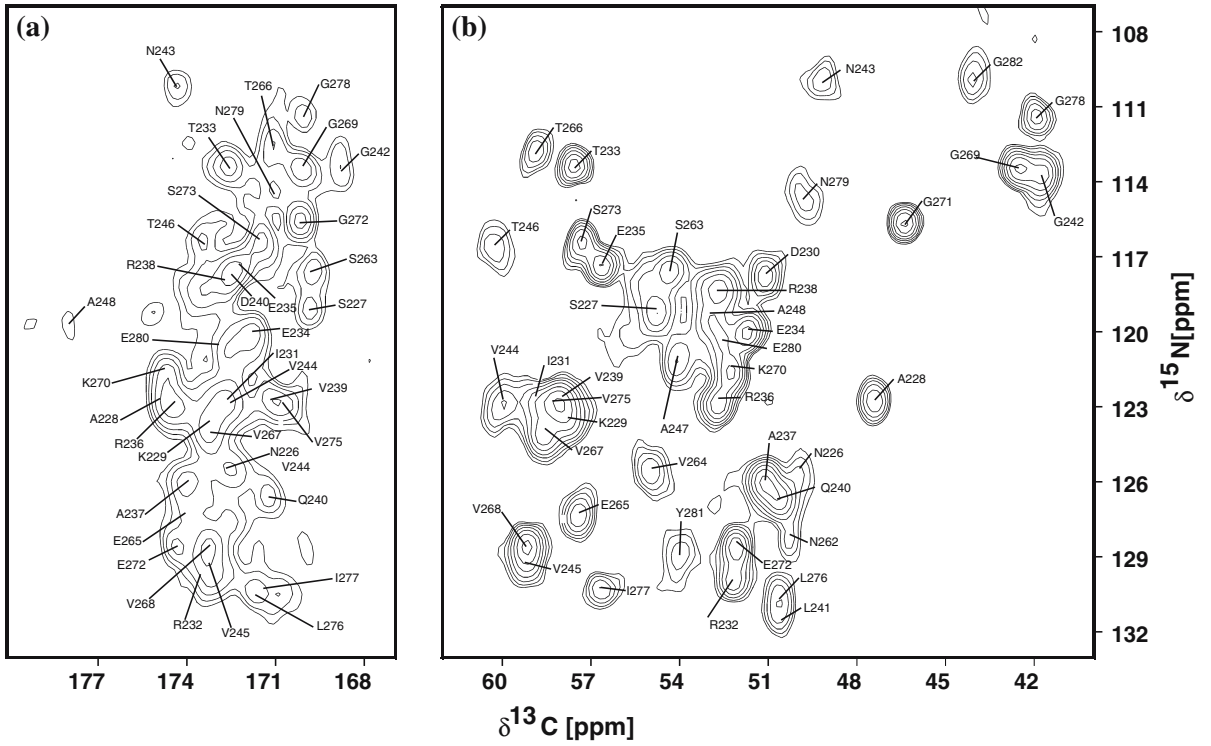

Figure 4. ^{15}N —^{13}C correlation spectra recorded at 40 kHz MAS. (a) N(CA)CO spectrum showing cross-peaks between the main-chain ^{15}N and the carbonyl of the same amino acid. Negative contours start at 20% of the minimum intensity. (b) NCA spectrum. Positive contours start at 9% of the maximum intensity.

was the low chemical-shift dispersion of the C′ resonances and the fact that there is no direct coherence between a N–C'_{i-1} correlation in the NCO spectrum and the corresponding C^{α}_{i-1} correlation in the N(CO)CA spectrum. Some of these ambiguities could be resolved in a three-dimensional NCOCA spectrum.

In order to confirm the assignment the CA–CA correlation spectrum shown in Figure 7 was recorded. The C^{α}_{i}—C^{α}_{i-1} cross-peaks of this spectrum confirmed the backbone assignment independently of the assignment of the backbone nitrogen resonance frequencies. As can be seen from Figure 7, all strong peaks could be explained as either C^{α}_{i}—C^{α}_{i-1} cross peaks or as diagonal peaks. The latter were not expected and their occurrence is not understood yet. Five of the cross peaks predicted from the assignment were not detected. All of them involve either glycine or arginine residues. Nevertheless, this spectrum was used as an important cross check of the assignment and confirms the information obtained from, the NCO, N(CO)CA, and NCOCA spectra. Due to the sequential nature of the polarization transfer in our implementation of the CA–CA experiment (Figure 1e), only $C^{\alpha}_{i} \rightarrow C^{\alpha}_{i-1}$ cross peaks can be observed. Diagonal peaks are also present, but with much smaller intensity as for example in PDSD spectra. PDSD spectra would in addition show $C^{\alpha}_{i} \rightarrow C^{\alpha}_{i+1}$ cross peaks leading to more overlap.

Extent of the assignment

Although the assignment presented in Table 1 explains most of the cross-peaks in Figures 3–7, only 43 of the 72 amino acids of the HET-s fragment 218–289 could be assigned. These amino acids are found in two fragments. The first of these fragments ranges from Asn226 to Ala248, the second from Asn262 to Gly282 with Arg274 missing. From these 43 amino acids 33 have a complete side-chain assignment.

The unobservable resonances form three ranges: at the N-terminus, at the C-terminus (including His tag), and in the middle of the investigated

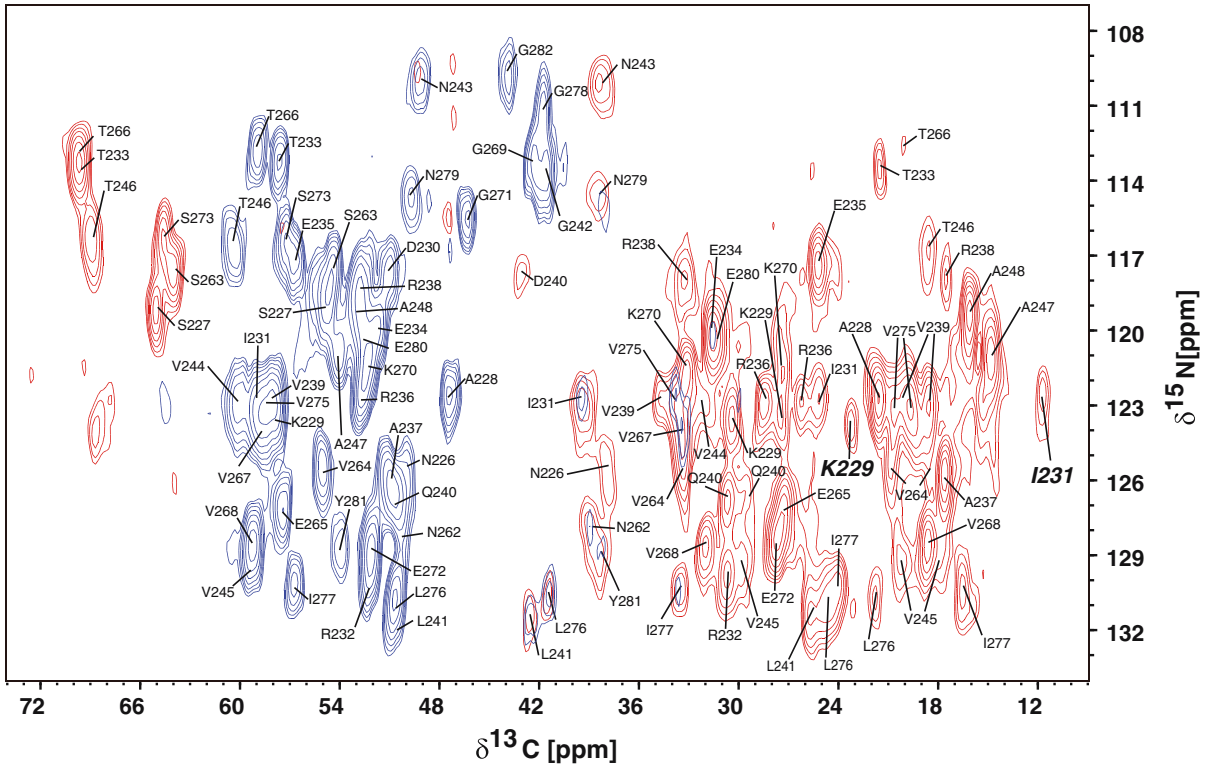

Figure 5. Superposition of the NCA and N(CA)CB spectrum recorded at 25 kHz MAS. The NCA experiment is shown here in blue, positive contours starting at 14% of the maximum intensity. The N(CA)CB spectrum is shown in red, negative contours starting at 9% of the minimum intensity. The two cross-peaks with large labels are Lys229 N—C^{γ} and Ile231 N—$C^{\delta 1}$.

HET-s fragment. Possible reasons for the undetectable signals could either be static disorder leading to broad lines due to chemical-shift dispersion or dynamic disorder leading to broad lines due to relaxation effects or interference between the dynamic process and rf irradiation or MAS. So far we cannot give a clear answer to the origin of the missing resonances but there are some indications in the spectra which suggest that both mechanisms are active. We observed some increase in line width towards the end of the assigned fragments indicating that there is disorder in these parts of the sample. This is illustrated by the C^{β}—C′ peaks of Ala247 and Ala248 as well as by the C^{α}—C′ cross peak of Gly282 in the DREAM spectrum shown in Figure 3a. For these residues C^{β} and the C^{α} shifts are still well defined and narrow while the C′ line is broadened hinting at a disordered chemical environment. The presence of dynamic processes of some side chains even in the assigned regions can be inferred from the fact that the line width of some of the ^{13}C lines increases only slowly with decreasing ^{1}H decoupling field strength. Interestingly, NOE presaturation gave significant signal enhancement on our samples. Variable temperature 1D ^{13}C spectra down to a sample temperature of −90 °C (Figure 8) showed additional peak intensities appearing in the aromatic region of the 1D carbon spectrum. Most of this intensity is attributed to the terminal His tag. Furthermore, we observed a general broadening of all resonances lines at lower temperatures which prevented the identification of potentially appearing new resonances, e.g., in the C^{α} and C^{β} region of a 2D PDSD spectrum at −90 °C (data not shown).

Conclusions

We have described the partial resonance assignment of a non-crystalline sample of the prion protein HET-s(218–289) in its amyloid form. Despite the macroscopic heterogeneity in the sample

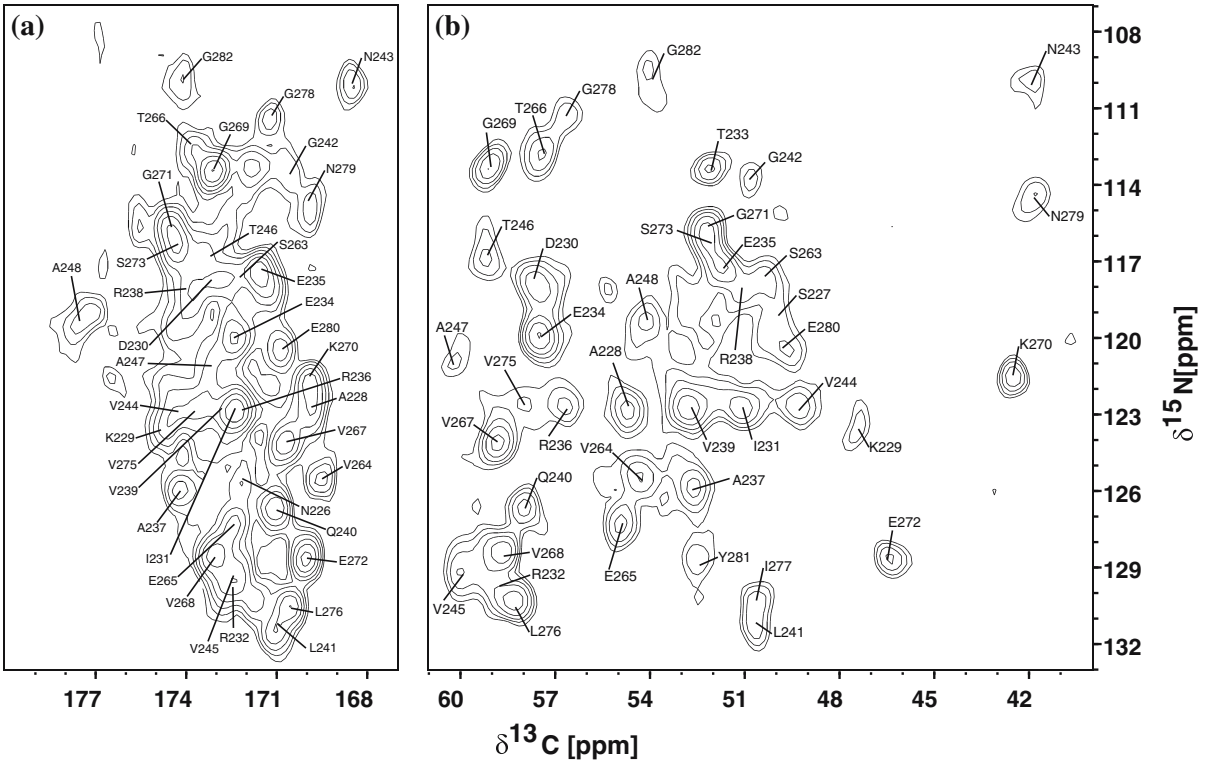

Figure 6. NCO and N(CO)CA spectra recorded at 40 kHz MAS. (a) NCO spectrum showing N_i—C'_{i-1} cross-peaks. Positive contours start at 18% of the maximum intensity. (b) N(CO)CA spectrum showing N_i—C^{α}_{i-1} cross-peaks. Negative contours start at 10% of the minimal intensity.

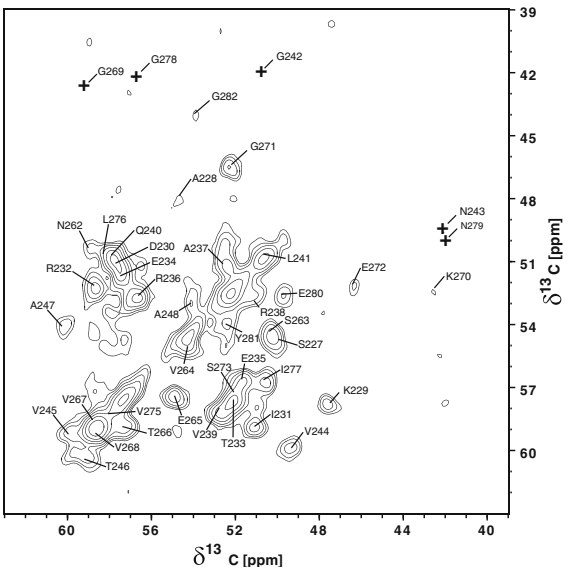

Figure 7. CA–CA spectrum recorded at 20 kHz MAS. Contours are shown starting at 10% of the maximal intensity. Assigned C^{α}_i—C^{α}_{i-1} cross peak are labelled by residue i. The positions of expected but absent C^{α}_i—C^{α}_{i-1} cross peaks are indicated with crosses.

as witnessed by electron microscopy, the NMR line width in the spectra was found to be comparable to microcrystalline samples, indicating that the structure is very regular on a molecular scale. We may speculate, that the highly regular fibril formation is connected to the biological role of the HET-s prion which could be evolutionary optimized while most of the system studied so far have been performed on fibrils that play a pathological role in nature (Ritter et al., 2005). The spectral assignment was done entirely *de novo* because the fact that the fragment adapts a random-coil conformation when dissolved prevents comparison with the liquid-state spectrum.

The assignment presented is based on experiments at high MAS frequencies (20–40 kHz), with correspondingly small sample volumes. Adiabatic schemes were applied for all polarization-transfer steps. High MAS frequencies are of advantage because of the better averaging of anisotropic interactions and the fact that the highly efficient homonuclear transfer schemes R^2T (for C'—C^{α}

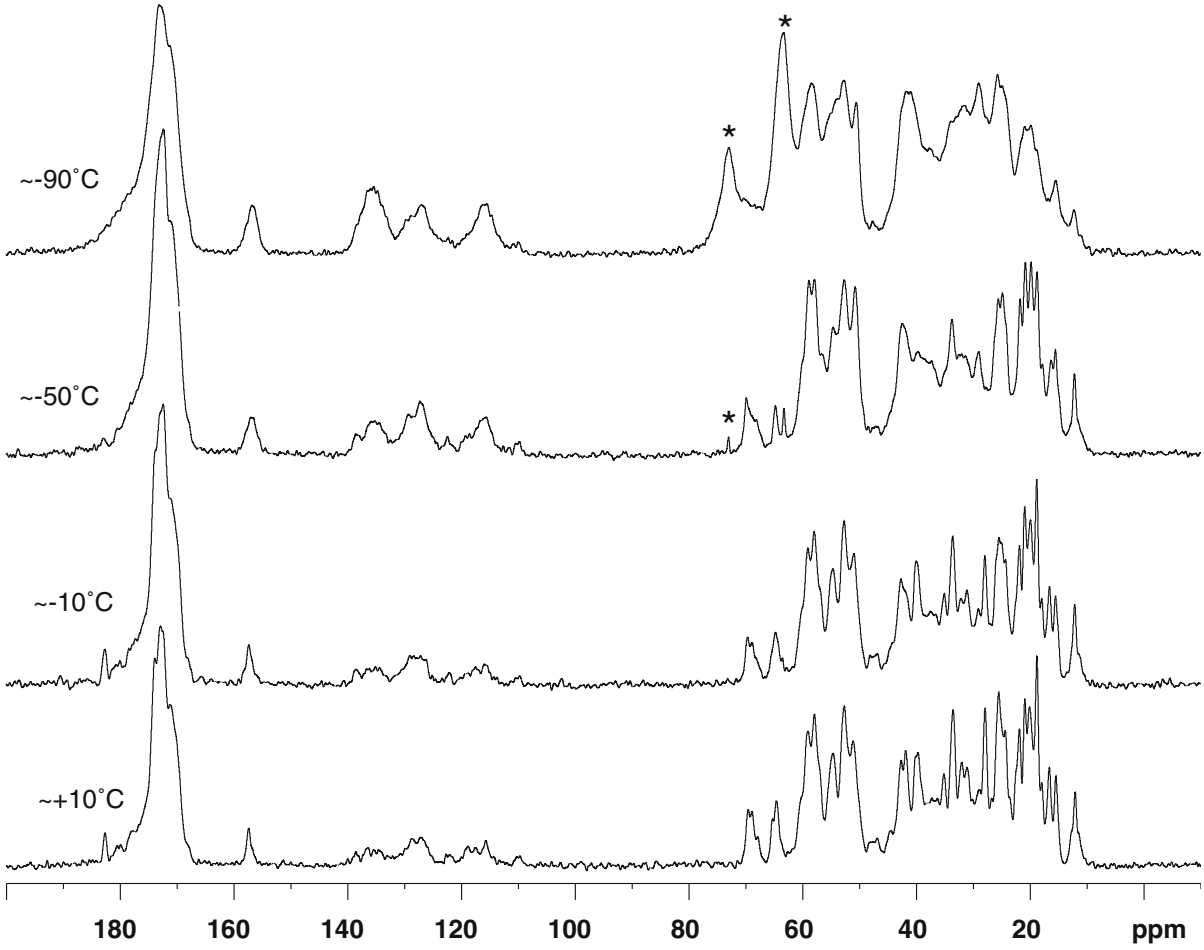

Figure 8. Temperature dependence of the 1D ^{13}C spectrum of HET-s(218–289). Spectra of fibrils dissolved in a water glycerol (1:1) mixture were recorded at 20 kHz MAS with 256 scans each. The glycerol peaks are indicated with stars.

transfer at 14.09 T) and DREAM become feasible (Ernst et al., 2003). Triple-resonance experiments with three transfer steps were performed on less than 14 mg of protein.

Although the HET-s(218–289) sample was not crystalline, more than half of the residues were very well structured giving rise to narrow lines. The solid-state resonance assignment revealed that these residues are located in two fragments of about 20 amino acids. The rest of the resonances were probably too broad or dynamic to be detected in our spectra. The chemical-shift analysis of the assigned residues gives some structural insights into the amyloid fibril. The two well-structured parts of HET-s(218–289) are mostly in a β-sheet conformation and the chemical shift of the residues assigned in this study can be used, in combination with proton/deuterium exchange experiments and solvent-accessibility studies, to obtain structural information about the protein and to correlate the structural information with infectivity (Ritter et al., 2005).

Electronic supplementary material is available at http://dx.doi.org/10.1007/s10858-005-5582-7.

Acknowledgement

We are grateful to Andreas Hunkeler and Urban Meier for technical support. We would like to thank Dr René Verel for stimulating discussion and Dr Andreas Detken for starting the preliminary research that lead to this paper. Financial support by the ETH Zurich, Swiss National Science Foundation and the National Institutes of Health is acknowledged.

References

Baldus, M., Geurts, D.G., Hediger, S. and Meier, B.H. (1996) *J. Magn. Reson. Ser. A*, **118**, 140–144.

Baldus, M. and Meier, B.H. (1996) *J. Magn. Reson. Ser. A*, **121**, 65–69.

Baldus, M., Petkova, A.T., Herzfeld, J. and Griffin, R.G. (1998) *Mol. Phys.*, **95**, 1197–1207.

Balguerie, A., Dos Reis, S., Ritter, C., Chaignepain, S., Coulary-Salin, B., Forge, V., Bathany, K., Lascu, I., Schmitter, J.-M., Riek, R. and Saupe, S.J. (2003) *EMBO J.*, **22**, 2071–2081.

Bennett, A.E., Ok, J.H., Griffin, R.G. and Vega, S. (1992) *J. Chem. Phys.*, **96**, 8624–8627.

Bockmann, A., Lange, A., Galinier, A., Luca, S., Giraud, N., Juy, M., Heise, H., Montserret, R., Penin, F. and Baldus, M. (2003) *J. Biomol. NMR*, **27**, 323–339.

Brinkmann, A., Eden, M. and Levitt, M.H. (2000) *J. Chem. Phys.*, **112**, 8539–8554.

Carravetta, M., Eden, M., Zhao, X., Brinkmann, A. and Levitt, M.H. (2000) *Chem. Phys. Lett.*, **321**, 205–215.

Castellani, F., van Rossum, B., Diehl, A., Schubert, M., Rehbein, K. and Oschkinat, H. (2002) *Nature*, **420**, 98–102.

Castellani, F., van Rossum, B.J., Diehl, A., Rehbein, K. and Oschkinat, H. (2003) *Biochemistry*, **42**, 11476–11483.

Costa, P.R., Sun, B.Q. and Griffin, R.G. (1997) *J. Am. Chem. Soc.*, **119**, 10821–10830.

Coustou-Linares, V., Maddelein, M.-L., Begueret, J. and Saupe, S.J. (2001) *Mol. Microbiol.*, **42**, 1325–1335.

Detken, A., Hardy, E.H., Ernst, M., Kainosho, M., Kawakami, T., Aimoto, S. and Meier, B.H. (2001) *J. Biomol. NMR*, **20**, 203–221.

Detken, A., Hardy, E.H., Ernst, M. and Meier, B.H. (2002) *Chem. Phys. Lett.*, **356**, 298–304.

Dos Reis, S., Coulary-Salin, B., Forge, V., Lascu, I., Begueret, J. and Saupe, S.J. (2002) *J. Biol. Chem.*, **277**, 5703–5706.

Earl, W.L. and VanDerHart, D.L. (1982) *J. Magn. Reson.*, **48**, 35–54.

Ernst, M., Detken, A., Bockmann, A. and Meier, B.H. (2003) *J. Am. Chem. Soc.*, **125**, 15807–15810.

Gammeren, A.J.v., Hulsbergen, F.B., Hollander, J.G. and Groot, H.J.M.d. (2005) *J. Biomol. NMR*, **31**, 279–293.

Glass, N.L., Jacobson, D. and Shiu, P. (1997) *Annu. Rev. Genet.*, **34**, 165–186.

Harris, R.K., Becker, E.D., Cabral de Menezes, S.M., Goodfellow, R. and Granger, P. (2002) *Magn. Reson. Chem.*, **40**, 489–505.

Hediger, S., Meier, B.H. and Ernst, R.R. (1995) *Chem. Phys. Lett.*, **240**, 449.

Hediger, S., Meier, B.H., Kurur, N.D., Bodenhausen, G. and Ernst, R.R. (1994) *Chem. Phys. Lett.*, **223**, 283–288.

Hong, M. (1999) *J. Biomol. NMR*, **15**, 1–14.

Igumenova, T.I., McDermott, A.E., Zilm, K.W., Martin, R.W., Paulson, E.K. and Wand, A.J. (2004) *J. Am. Chem. Soc.*, **126**, 6720–6727.

Igumenova, T.I., Wand, A.J. and McDermott, A.E. (2004) *J. Am. Chem. Soc.*, **126**, 5323–5331.

Ishii, Y. and Tycko, R. (2000) *J. Am. Chem. Soc.*, **122**, 1443–1455.

Jaroniec, C.P., MacPhee, C.E., Bajaj, V.S., McMahon, M.T., Dobson, C.M. and Griffin, R.G. (2004) *PNAS*, **101**, 711–716.

Keller, R.L.J. (2004) *The Computer Aided Resonance Assignment Tutorial*, Cantina Verlag, Goldau.

Lange, A., Becker, S., Seidel, K., Giller, K., Pongs, O. and Baldus, M. (2005) *Angew. Chem.-Int. Edit.*, **44**, 2089–2092.

Maddelein, M.L., Dos Reis, S., Duvezin-Caubet, S., Coulary-Salin, B. and Saupe, S.J. (2002) *Proc. Natl. Acad. Sci. U.S.A*, **99**, 7402–7407.

Marion, D. and Wuthrich, K. (1983) *Biochem. Biophys. Res. Commun.*, 967–974.

Morcombe, C.R. and Zilm, K.W. (2003) *J. Magn. Reson.*, **162**, 479–486.

Pauli, J., Baldus, M., van Rossum, B., de Groot, H. and Oschkinat, H. (2001) *Chembiochem*, **2**, 272–281.

Petkova, A.T., Baldus, M., Belenky, M., Hong, M., Griffin, R.G. and Herzfeld, J. (2003) *J. Magn. Reson.*, **160**, 1–12.

Petkova, A.T., Buntkowsky, G., Dyda, F., Leapman, R.D., Yau, W.M. and Tycko, R. (2004) *J. Mol. Biol.*, **335**, 247–260.

Rienstra, C.M., Hohwy, M., Hong, M. and Griffin, R.G. (2000) *J. Am. Chem. Soc.*, **122**, 10979–10990.

Ritter, C., Maddelein, M.L., Siemer, A.B., Luhrs, T., Ernst, M., Meier, B.H., Saupe, S.J. and Riek, R. (2005) *Nature*, **435**, 844–848.

Samoson, A., Tuherm, T., Past, J., Reinhold, A., Anupold, T. and Heinmaa N. (2005) *In New Techniques in Solid-State NMR*, Vol. 246, pp. 15–31.

Saupe, S.J. (2000) *Microbiol. Mol. Biol. Rev.*, **64**, 489–502.

Straus, S.K., Bremi, T. and Ernst, R.R. (1998) *J. Biomol. NMR*, **12**, 39–50.

Takegoshi, K., Nomura, K. and Terao, T. (1995) *Chem. Phys. Lett.*, **232**, 424–428.

Takegoshi, K., Nomura, K. and Terao, T. (1997) *J. Magn. Reson.*, **127**, 206–216.

Tycko, R. (2004) *Curr. Opin. Struct. Biol.*, **14**, 96–103.

van Rossum, B.J., Castellani, F., Pauli, J., Rehbein, K., Hollander, J., de Groot, H.J.M. and Oschkinat, H. (2003) *J. Biomol. NMR*, **25**, 217–223.

Verel, R., Baldus, M., Ernst, M. and Meier, B.H. (1998) *Chem. Phys. Lett.*, **287**, 421–428.

Verel, R., Ernst, M. and Meier, B.H. (2001) *J. Magn. Reson.*, **150**, 81–99.

Zech, S.G., Wand, A.J. and McDermott, A.E. (2005) *J. Am. Chem. Soc.*, **127**, 8618–8626.